Table 2 – Protein increased in HNSCC.

Protein increased in tumor tissue												
Spot no. [a]	Database accession no.	Unit ProtKB accession no.	Protein name	Average mass	Score	Seq. cov. (%) [b]	MS/MS (unique) [c]	Fold increase	Standard deviation	t-test	Pretension mass	References [e]
T1	gi-4507651	P67936	Tropomyosin 4	28,504	147	14	4	1.98	0.95	<0.001	33,000	(1)
T2	gi-187302	P31947	Epithelial cell marker protein 1	27,759	152	19	5	2.57	2.26	<0.001	31,000	(1,2)
T3	gi-49119653	P63104	YWHAZ protein	29,929	191	18	4	1.50	0.30	<0.001	31,000	(2)
T4	gi-16507237	P11142	Heat shock 70 kD protein 5	72,288	683	28	18	1.57	0.78	0.096	85,000	(3)
T5	gi-1199487	P50454	Collagen binding protein 2	46,506	245	22	8	4.54	1.95	<0.001	46,000	
T6	gi-45604447	P22626	Heterogeneous nuclear ribonucleoprotein A2/B1	35,984	145	14	3	2.01	1.00	0.015	34,000	
T7	gi-4505591	Q06830	Perox iredoxin 1	22,096	116	22	4	1.85	0.81	<0.001	23,000	(4)
T8	gi-62738525	P36952	Serpin	42,615	328	26	8	1.65	1.04	0.042	40,000	(5)
T9	gi-4503471	P68104	Eukaryotic translation elongation factor 1 alpha 1	50,109	215	11	5	5.39	2.79	<0.001	47,000	
T10	gi-42544159	Q92598	Heat shock 105 kD	96,804	329	10	8	1.52	0.56	0.028	110,000	
T11	gi-4504165	P06396	Gelsolin	85,644	286	10	6	1.52	0.41	0.018	90,000	(7)
T12	gi-10863945	P13010	ATP-dependent DNA helicase II	82,652	201	12	7	2.56	1.64	<0.001	880,000	
T13	gi-4507115	Q16658	Fascin 1	54,496	104	7	3	2.41	2.07	0.004	51,000	(8)
T14	gi-5031573	P61158	Actin-related protein 3	47,341	148	11	4	4.90	4.66	0.008	48,000	(8)
T15	gi-4503445	P19971	Endothelial cell growth factor 1 precursor	49,924	486	25	12	2.67	1.41	0.014	51,000	
T16	gi-30130	P50454	Collagen	46,238	97	6	2	3.25	2.74	0.013	47,000	(9)
T17	gi-75517570	P09651	HNRPA 1 protein	29,368	306	33	7	2.50	1.71	0.025	33,000	
T18	gi-181967	P68104	Elongation factor 1-alpha	35,205	52	3	1 [d]	1.93	1.00	0.075	32,000	
T19	gi-49168580	P40926	MDH2	35,537	613	46	15	3.02	4.53	0.031	34,000	
T20	gi-4557032	P07195	Lactate dehydrogenase B	36,615	213	20	6	1.53	0.54	0.006	33,000	
T21	gi-18645167	P07355	Annexin A2	38,552	177	18	5	4.57	5.05	<0.001	3200	(10)
T22	gi-37724561	P63244	Lung cancer oncogene 7	37,865	181	11	3	3.03	4.85	0.016	32,000	
T23	gi-48255905	Q01995	Transgelin	22,596	151	29	5	2.60	1.55	<0.001	25,000	
T24	gi-4504517	P04792	Heat shock 27 kDa protein 1	22,768	261	31	5	1.57	0.34	<0.001	30,000	(1)
T25	gi-47939618	P09651	Heterogeneous nuclear ribonucleoprotein A1	34,159	202	13	4	6.48	7.41	<0.001	32,000	
T26	gi-31542947	P10809	Chaperonin	61,016	496	34	16	2.08	1.70	0.01	62,000	(11)
T27	gi-31542947	P30101	ER0-60 protease	56,761	427	23	14	1.83	0.87	0.044	60,000	
T28	gi-320200	Q00839	Scaffold attachment factor A	90,423	427	11	8	2.59	1.37	0.009	120,000	
T29	gi-63252900	P09493	Tropomyosin 1 alpha chain	32,856	205	20	7	2.59	1.80	0.025	33,000	(11)
T30	gi-68533131	Q4LE33	TNC variant protein	244,248	2222	20	41	3.98	1.91	0.009	250,000	
T31	gi-41322908	Q15149	Plectin 1	513,393	503	5	20	1.69	0.64	0.035	30,000	

[a] Spot numbers refer to those in Fig. 1.
[b] Amino acid sequence coverage for the identified protein.
[c] Number of peptide fragments of a protein that yielded informative MS/MS data (number of unique peptide). The minimum criterion of the probability-based MASCOT/MOWSE score was set with 5% as the significant threshold level
[d] MS/MS spectrum refers to Fig. S2.
[e] The references are listed in Supplementary Information 3.

JOURNAL OF PROTEOMICS 75 (2012) 1803–1815

Table 3 – Protein decreased in HNSCC.

Protein decreased in tumor tissue												
Spot no. [a]	Database accession no.	Unit ProtKB accession no.	Protein name	Average mass	Score	Seq. cov. (%) [b]	MS/MS (unique) [c]	Fold decrease	Standard deviation	t-test	Pretension mass	References [d]
N1	gi-4502101	P04083	Annexin I	38,690	336	21	8	7.49	7.59	<0.001	39,000	(12)
N2	gi-4557871	P02787	Transferrin	77,000	259	11	7	5.13	3.07	<0.001	83,000	(13)
N3	gi-177831	P01009	Alpha-1-antitrypsin	46,677	252	21	8	6.18	4.08	<0.001	66,000	(2)
N4	gi-7706635	Q9UBG3	Cornulin	53,502	244	18	5	7.10	6.06	<0.001	66,000	(3)
N5	gi-179106	Q13813	Nonerythroid alpha-spectrin	284,107	648	11	24	1.81	0.81	0.014	220,000	
N6	gi-2992541	O60437	Periplakin	204,580	975	22	35	4.32	3.02	<0.001	182,000	
N7	gi-27436946	P02545	Lamin A/C	74,095	450	21	13	2.16	1.18	<0.001	81,000	(14)
N8	gi-119589476	P01024	Complement component 3	143,619	347	9	9	2.81	1.83	0.005	70,000	
N9	gi-37267	P29401	Transketolase	67,751	169	11	6	4.05	4.11	0.016	68,000	
N10	gi-340219	P08670	Vimentin	53,681	382	29	14	2.15	1.96	0.005	48,000	
N11	gi-40647126	P01860	Anti-HIV-1 gp120 immunoglobulin	22,899	54	11	2	4.96	5.15	0.014	52,000	(1,2)
N12	gi-12798841	P25705	ATP synthase	59,671	100	6	3	5.18	5.32	0.038	53,000	(11)
N13	gi-297412	P35237	Thrombin inhibitor	42,559	69	6	2	2.61	1.75	0.008	43,000	
N14	gi-178775	P02647	Propolipoprotein	28,944	187	21	5	4.58	2.14	<0.001	25,000	
N15	gi-4504517	P04792	Heat shock 27 kDa protein 1	22,768	279	33	7	1.72	0.62	<0.001	31,000	(1)
N16	gi-149673887	P01834	Immumoglobulin lights chain	23,331	109	17	2	2.44	1.15	<0.001	30,000	(1)
N17	gi-4502517	P00915	Carbonic annhydrase I	28,852	249	31	7	2.41	1.25	0.016	32,000	(2)
N18	gi-34234	P08865	Laminin-binding protein	31,774	141	14	3	5.16	10.01	0.004	44,000	(2)
N19	gi-87196339	P12109	Collagen type VI, alpha 1 precursor	108,462	319	10	9	3.52	5.06	<0.001	120,000	
N20	gi-41350923	P12110	Collagen type VI, alpha 2	108,539	151	5	4	3.43	4.91	0.026	120,000	
N21	gi-1147813	P15924	Desmoplakin I	331,571	190	3	7	2.45	2.08	0.043	220,000	(15)
N22	gi-4503483	P13639	Eukaryotic translation elongation factor 2	95,277	91	3	3	4.23	5.40	0.042	97,000	(15)
N23	gi-136066	P060174	Triosephosphate isomerase	26,609	432	38	7	2.58	1.60	<0.001	30,000	
N24	gi-14194715	Q92817	Envoplakin	231,477	110	1	2	2.52	2.24	0.007	20,0000	
N25	gi-860986	P07237	Protein disulfide-isomerase	56,644	141	8	5	2.10	1.63	0.061	47,000	(13)
N26	gi-13489087	P30740	Serine proteinase inhibitor	42,715	427	34	11	3.37	2.84	<0.001	41,000	(14)
N27	gi-4507877	P18206	Vinculin	116,649	177	6	7	1.93	0.71	<0.001	100,000	
N28	gi-55743104	P12111	Alpha 3 type VI collagen precursor	321,987	421	5	17	2.05	1.55	0.013	190,000	
N29	gi-5729877	P11142	Heat shock 70 kDa protein 8	70,854	156	7	4	4.76	4.74	0.004	62,000	(3)
N30	gi-386785	P08107	Heat shock protein	69,825	462	19	12	3.14	2.46	0.005	61,000	
N31	gi-157671915	Q6ZN66	Guarrylate binding protein 6	72,381	65	3	2	2.85	1.71	0.002	61,000	(3)
N32	gi-61743954	Q09666	AHNAK nucleoprotein	628,699	323	3	15	2.44	1.98	0.014	260,000	
N33	gi-124731	P07476	AHNAK nucleoprotein	68,427	218	15	7	2.16	1.35	0.003	115,000	
N34	gi-492570004	P13928	Annexin A8	36,872	69	6	2	3.66	2.71	0.035	35,000	(2)

[a] Spot numbers refer to those in Fig. 1.

[b] Amino acid sequence coverage for the identified protein.

[c] Number of peptide fragments of a protein that yielded informative MS/MS data (number of unique peptide). The minimum criterion of the probability-based MASCOT/MOWSE score was set with 5% as the significant threshold level.

[d] The references are listed in Supplementary Information 3.

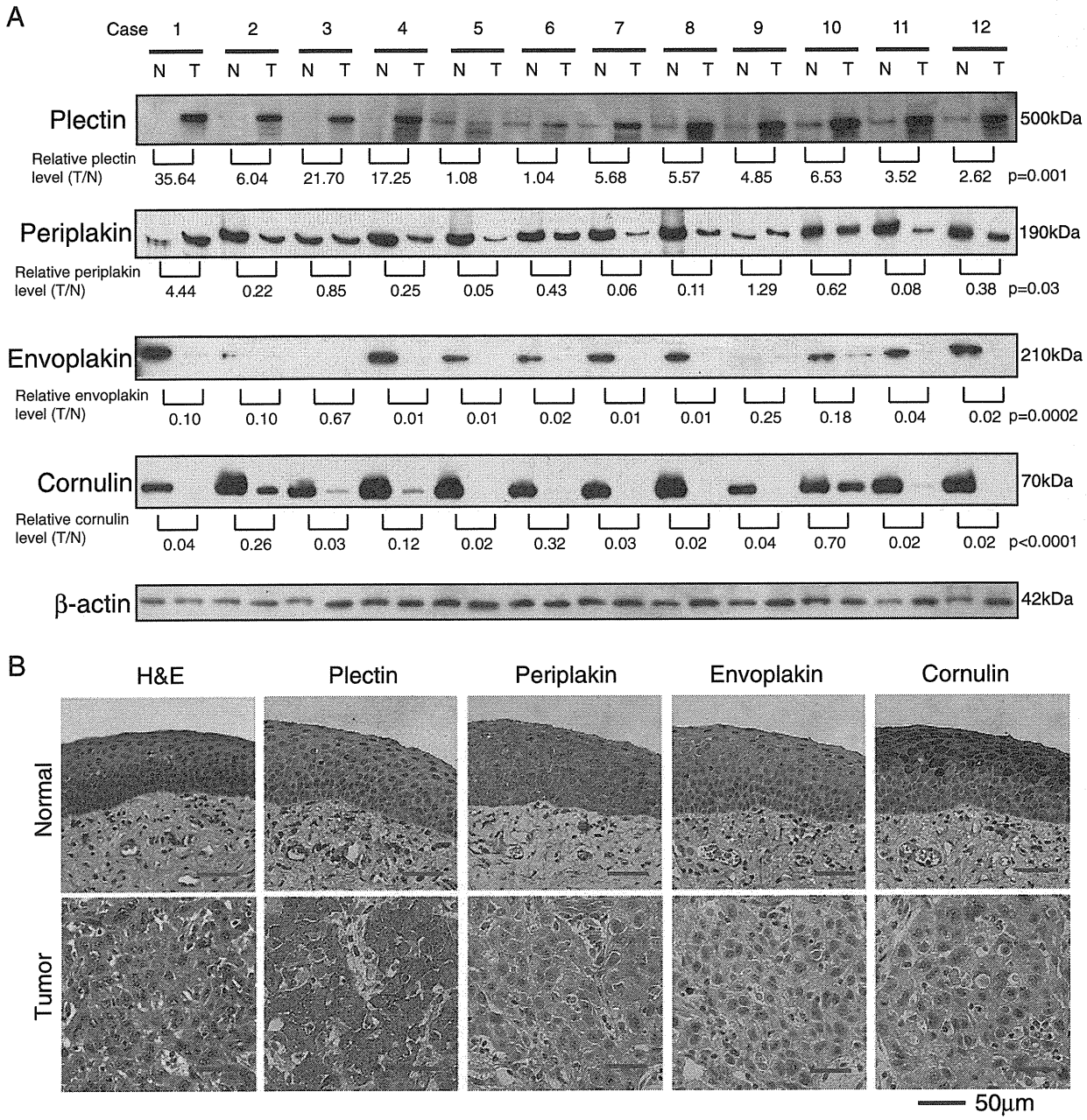

Fig. 2 – Validation of differentially expressed proteins in HNSCC tissues by Western blotting and immunohistochemistry. A, Western blots of total protein lysates prepared from twelve matched samples of tumor (T) and adjacent non-tumor tissue (N) with anti-plectin, anti-periplakin, anti-envoplakin, anti-cornulin, and anti-β-actin antibodies (loading control). The intensity of each band was measured with TotalLab™ 1D software (Nonlinear Dynamics, Newcastle upon Tyne, UK), and protein levels were calculated between tumor and non-tumor tissue, normalized with β-actin. The difference in protein expressions between (T) and (N) was assessed by Student's t-test for unpaired values. B, Immunohistochemical analysis of paraffin-embedded normal epithelia and cancer tissues with plectin, periplakin, envoplakin, and cornulin antibodies. HE: hematoxylin and eosin.

of Erk 1/2 kinases was significantly elevated in plectin−/− keratinocytes and was the cause of the faster migration of plectin-deficient cells. Upregulation of Erk 1/2 kinases has been shown to play a role in tumor invasion by inducing EMT [16], or by promoting the degradation of extracellular matrix proteins through induction of MMPs [17,18]. Furthermore, overexpression of N-cadherin induces cell migration in vitro and invasion and metastasis in vivo by an Erk 1/2-dependent mechanism [19,20]; therefore, we investigated Erk 1/2 activities in plectin knockdown HNSCC cells. Surprisingly, phosphorylated Erk 1/2 was significantly decreased in plectin siRNA-treated cells as compared with control siRNA-treated

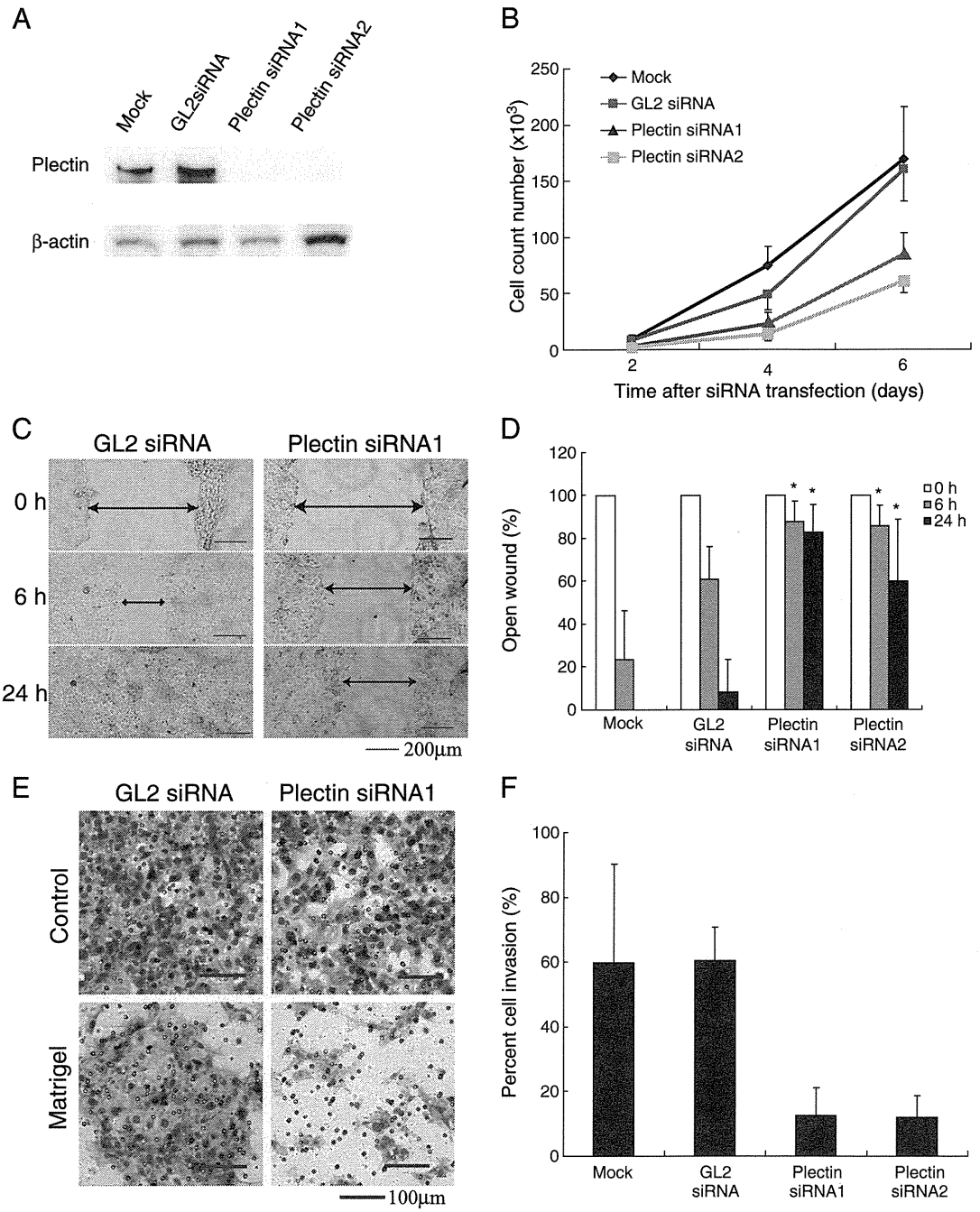

Fig. 3 – Suppression of plectin inhibits the cell proliferation, migration, and invasion of HNSCC cells. A, Expression of plectin in D562 cells was determined by Western blotting 24 hrs after plectin siRNA treatment. GL2 siRNA was used as a control. β-actin was used as a control for internal protein loading. B, Knockdown of plectin expression by siRNA significantly suppresses the proliferation of D562 cells. Cells were transfected with Mock, GL2siRNA, plectin siRNA1 and −2. Cells were cultured for the indicated time. *, $P<0.05$, control siRNA compared with siRNAs. C and D, Suppression of plectin decreased cancer cell migration. Cells were scratched with a pipette tip and migration toward the wounded area was observed. *, $P<0.05$, control siRNA compared with plectin siRNA. E, Suppression of plectin decreased cancer cell invasion. Representative images show cells that passed through the control chamber or Matrigel when transfected with control and plectin siRNA1. F, Three randomly selected fields were photographed and the number of invaded cells was counted. Percent cell invasion was calculated as the mean number of cells passing through a Matrigel insert membrane relative to passing through a control insert membrane. *, $P<0.05$, control siRNA compared with plectin siRNAs.

cells (Fig. 4A,B). Total Erk 1/2 level was also slightly decreased in plectin siRNA-treated cells (Fig. 4A,B). Although the relationship between plectin expression and Erk 1/2 activity remains obscure, these results suggest that the inhibition of migration and invasion in plectin knockdown cells may be associated with downregulation of Erk 1/2 kinase activities,

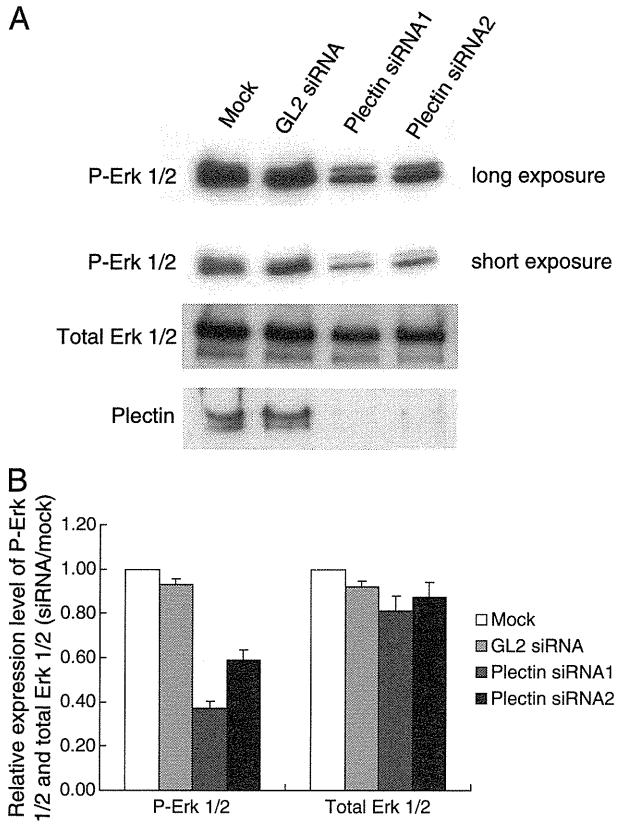

Fig. 4 – Suppression of plectin attenuates phosphorylated Erk 1/2 level. A. Expression of phosphorylated Erk 1/2 (P-Erk 1/2) and total Erk 1/2 in D562 cells was examined by Western blotting 24 hrs after plectin siRNA treatment. GL2 siRNA was used as a control. B. The intensity of P-Erk 1/2 and total Erk 1/2 bands in siRNA-treated cells were measured with TotalLab TL120 and the relative expression levels of each protein as compared with mock treatment are shown.

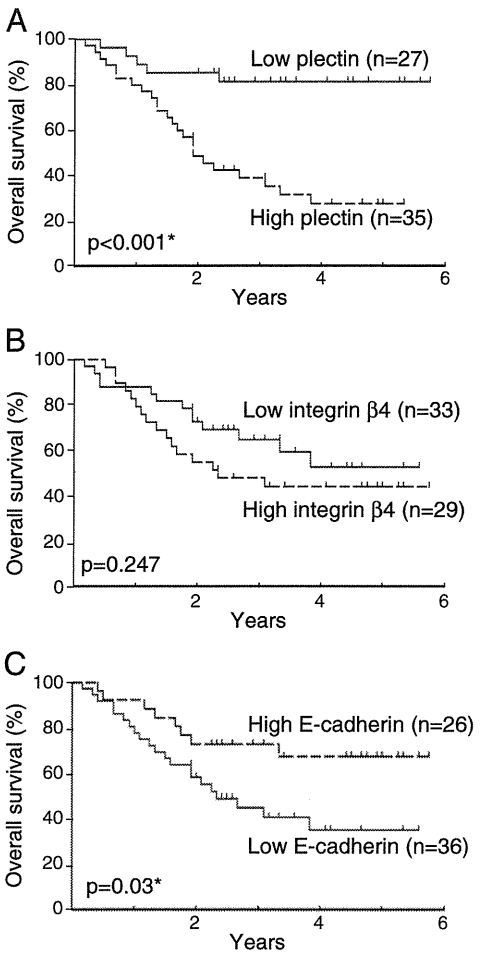

Fig. 5 – Kaplan-Meier survival curves according to expression levels of plectin (P<0.001; A), integrin β4 (P=0.247; B), and E-cadherin (P=0.03; C) in HNSCC.

which explains the different migration behavior between plectin-deficient keratinocytes and HNSCC cells.

3.5. *Plectin is a potential prognostic marker of HNSCC*

The above experiments strongly imply that upregulation of plectin is involved in metastasis and, as a result, the malignant potential of HNSCC. For this reason, we next examined whether plectin is associated with the prognosis of HNSCC patients. Immunohistochemistry of paraffin-embedded tissues obtained from 62 HNSCC patients was performed using anti-plectin antibody and its expression level was judged on a scale of 0 to 3+: 0, no staining; 1+, weak staining; 2+, moderate staining; 3+, strong staining (Fig. S1A). For statistical analysis, scores of 0 and 1+ were rated as low expression, and scores of 2+ and 3+ were rated as high expression. Survival curves were calculated by the Kaplan-Meier method and analyzed using the log-rank test. Strikingly, the survival rate of patients with a higher plectin level (≥2+) was significantly decreased ($P<0.001$) (Fig. 5A).

To test if the correlation of the survival rate and plectin expression level is comparable to other well-known prognosis markers of HNSCC, we analyzed the survival rate according to the expression levels of integrin β4 and E-cadherin, which were previously reported to correlate with the clinical outcomes of HNSCC patients [21-24]. Integrin β4 and E-cadherin expression levels were examined by IHC and judged on a scale of 0 to 3+ according to the intensity of staining (Fig. S1B, C). The results showed that a high expression of integrin β4 was not correlated with the poor prognosis of HNSCC patients ($P=0.247$, log-rank test) (Fig. 5B). Moreover, although a low expression of E-cadherin was correlated with the poor prognosis of HNSCC patients ($P=0.03$, log-rank test), its P value was much higher than that of statistical analysis by plectin expression (Fig. 5C). These results strongly indicate that plectin is a promising prognostic marker for HNSCC.

We further investigated whether the expression levels of plectin, integrin β4, and E-cadherin in cancer cells correlated with the clinical outcomes of HNSCC patients (Table 4). There was no significant correlation between plectin, integrin β4, or E-cadherin expression and gender, age, location of tumors, histology, clinical stage, or local recurrence; significant correlation was only observed between the plectin expression level and with or without distant metastasis in HNSCC patients. This result further supports the idea that plectin is involved in the metastasis and malignant potential of HNSCC.

Table 4 – Characteristics of 62 HNSCC patients in IHC analysis.

		Plectic-IHC expression			Integrin β4-IHC expression			E-cadherin-IHC expression		
	Total (62)	Low (27)	High (35)	P	Low (33)	High (29)	P	Low (36)	High (26)	P
Gender										
Male	50	21	29		27	23		31	19	
Female	12	6	6	NS	6	6	NS	5	7	NS
Age										
≧60	39	17	22		23	16		22	17	
<60	23	10	13	NS	10	13	NS	14	9	NS
Location of tumors										
Oral	23	11	12		14	9		12	11	
Oropharynx	2	1	1		1	1		2	0	
Hypopharynx	29	12	17		12	17		16	13	
Larynx	6	2	4		5	1		4	2	
Salivary gland	2	1	1	NS	1	1	NS	2	0	NS
Histology										
Well	18	10	8		12	6		7	11	
Moderate	38	14	24		19	20		26	12	
Poorly	6	3	3	NS	3	3	NS	3	3	NS
UICC-Stage										
I-III	17	10	7		12	5		9	8	
VI	45	17	28	NS	21	24	NS	27	18	NS
Local recurrence										
Yes	11	3	8		5	6		8	3	
No	51	24	27	NS	28	23	NS	28	23	NS
Distant metastasis										
Yes	25	7	18		14	11		15	10	
No	37	20	17	0.042	19	18	NS	21	16	NS

*Significance value $P<0.05$
NS, not significant

3.6. *Plectin is an independent prognostic marker of HNSCC*

Finally, we analyzed whether the plectin expression level was an independent clinical outcome factor in HNSCC patients. On univariate analysis, the clinical stage, plectin expression and E-cadherin expression were correlated with the overall survival time (Table 5, left). Furthermore, among these factors, the clinical stage (hazard ratio, 3.403; 95% confidence interval, 1.024–11.309, $P=0.0456$), plectin expression (hazard ratio, 5.519; 95% confidence interval, 1.653–18.433, $P=0.0055$) and E-cadherin expression (hazard ratio, 0.418; 95% confidence interval, 0.184–0.950, $P=0.0373$) were independent clinical outcome factors on multivariate analysis (Table 5, right). The data strongly suggested that plectin alone might be a prognostic biomarker of HNSCC.

4. Discussion

In this study, we searched for proteins that could serve as biomarkers for cancer diagnosis, prognosis, and therapeutic targets in HNSCC by agarose 2D-DIGE using surgically resected clinical specimens, and succeeded in identifying and validating several proteins that were differentially expressed in HNSCC. Among them, plectin was significantly overexpressed in HNSCC. Strikingly, HNSCC patients with a high plectin level suffered recurrence more frequently than those with a low plectin expression; as a result, the survival rate of patients with a high plectin level significantly declined. Furthermore, functional studies implied that a decreased expression of plectin suppresses the proliferation, migration and invasion of HNSCC cells. This is probably due to the downregulation of Erk 1/2 kinase activity in the cells, although whether it is caused by attenuated expression of plectin or by some other mechanism is unclear. These results provided evidence that plectin is a novel and promising prognostic biomarker of HNSCC.

Our results indicated that patients with a higher plectin level showed a much lower overall survival rate than those with a lower plectin level (Fig. 5). This difference in the survival rate is probably related with the higher metastatic potential of HNSCC with an increased plectin level (Table 4), which was supported by our experimental data and previous studies indicating that plectin is involved in cell migration and invasion. We showed that the suppression of endogenous plectin inhibited the migration and invasion of HNSCC cells (Fig. 3). In other studies, ablation of plectin impaired the migration of MCF-7 (human breast adenocarcinoma cell line) epithelial sheets [25]. Moreover, plectin interacts with the integrin β4, a receptor for laminins, which is a major component of the epidermal basement membrane [26]. Integrin β4 has been reported to associate with cell migration and invasion [12-14]. Furthermore, its high expression is associated with poor prognosis in a variety of human cancers [27,28]. Thus, overexpression of plectin might contribute to cell migration and invasion in HNSCC cells through its association with integrin β4.

On the other hand, Osmanagic-Myers et al. showed opposite results that suppression of plectin accelerates the

Table 5 – Prognostic factors by univariate and multivariate analysis.

Variables	Univariate analysis		Multivariate analysis	
	Hazard ratio 95% confidence interval	P	Hazard ratio 95% confidence interval	P
Gender (Male/Female)	0.608 (0.211-1.750)	0.3560		
Age (<60/≥60)	1.087 (0.505-2.340)	0.8312		
Location of tumors (larynx, pharynx/others)	0.494 (0.218-1.122)	0.0921		
WHO histological type (poor-moderate/well)	2.402 (0.913-6.325)	0.0759		
Clinical stage (I-III/VI)	4.471 (1.351-14.801)	0.0142*	3.403 (1.024-11.309)	0.0456*
Plectin (high/low)	6.359 (1.918-21.078)	0.0025*	5.519 (1.653-18.433)	0.0055*
Integrin β4 (high/low)	1.538 (0.739-3.204)	0.2498		
E-cadherin (low/high)	0.416 (0.184-0.942)	0.0355*	0.418 (0.184-0.950)	0.0373*

*Significance value $P<0.05$.

migration of keratinocytes [15]. How can this contradiction be explained? In keratinocytes, a MAP kinase Erk 1/2, which is known to positively regulate keratinocyte migration [29], was activated when plectin was depleted. This result was in marked contrast with our result that phosphorylated Erk 1/2 was down-regulated in plectin-deficient HNSCC cells. Ding et al. also reported that knockdown of plectin with RNA interference (RNAi) attenuates the activation of Erk1/2 in HEK293 cells [30]. The above results suggest that the effect on migration in plectin-deficient cells depends on the different response of Erk 1/2 activity to the alteration of plectin expression in each cell line.

Another mechanism of plectin-mediated migration and invasion might be its association with CXCR4 through the plectin N-terminal domain [30]. CXCR4 is the chemokine receptor for SDF-1 and has been reported to not only be expressed in a wide variety of carcinomas [31-34], but to be correlated with distant metastasis and poor prognosis in HNSCC [35]. Moreover, SDF-1/CXCR4 interaction is known to be involved in cell proliferation, migration, and invasion evoked through Erk 1/2 in several cancer cells [36-40]. This interaction and signal system may be related to the poor prognosis of HNSCC with high plectin expression.

We also observed that suppression of plectin inhibited the proliferation of HNSCC cells (Fig. 3), which suggests that plectin is involved in cancer development. In fact, overexpression of plectin has been previously reported in prostate cancer, colorectal cancer, and pancreatic cancer [41-43], although the precise mechanism of how plectin overexpression is related to cancer development is not clear. Plectin is a large protein that links intermediate filaments to microtubules and microfilaments, anchoring the cytoskeleton to the plasma and nuclear membranes [44,45]. It also plays important roles in signal transduction, is involved in Rho/Rac/Cdc42 signaling cascades [46] and is an early substrate for caspase 8 following apoptosis induction by CD95 or tumor necrosis factor receptor [47]. Thus, upregulation of plectin in HNSCC may have an impact on the signaling pathways that regulate cell migration and apoptosis.

Postoperative adjuvant therapy for HNSCC is now applied on the basis of the results of pathological examination of the surgical specimens (multiple lymph node metastases, extralymphatic invasion, a positive stump after microscopic resection). Efficacy of chemoradiotherapy as compared with radiotherapy alone was evaluated in two randomized trials conducted in Europe (European Organization Research and Treatment of Cancer; EORTC) and the United States (Radiation Therapy Oncology Group; RTOG) [48,49]. Although EORTC study revealed that chemoradiotherapy significantly increased overall survival without a high incidence of adverse effects, RTOG trial showed not only a marginal improvement of overall survival but significant increase in severe adverse effects with chemoradiotherapy. Inconsistencies emerged from these reports emphasizes an intense need to define more precise boundaries demarcating risk levels for the decision-making processes of adjuvant treatment [50]. Therefore, while chemotherapy combined with radiotherapy are effective as postoperative adjuvant therapies for HNSCC, better biomarkers to select patients with proper indications are necessary to practically improve the clinical outcome of the patients and/or prevent a risk of adverse effects of the treatment. In this regard, plectin could be a useful biomarker for more effective postoperative treatment options, such as radiation alone for patients with a low plectin level and radiation in combination with chemotherapy for patients with a high plectin level.

In summary, we identified plectin as a promising prognostic biomarker in HNSCC, which could make significant contributions to the prediction of HNSCC patient prognosis and might improve their clinical outcome through postoperative follow-up and additional therapy. Further investigation is needed to uncover the mechanisms responsible for plectin-mediated development of HNSCC.

Supplementary materials related to this article can be found online at doi:10.1016/j.jprot.2011.12.018.

Disclosure

The authors declare no conflicts of interest.

Acknowledgments

We would like to thank Masumi Ishibashi and Takahiro Kazami for their technical assistance. This work is supported

by Grants-in-Aid 18014007, 18659363, 19390330, 20014003 to T.T and 19390154 to F.N from the Ministry of Education, Science, Sports and Culture of Japan.

REFERENCES

[1] Jemal A, Siegel R, Ward E, Hao Y, Xu J, Thun MJ. Cancer statistics, 2009. CA Cancer J Clin 2009;59:225–49.

[2] Gold KA, Lee HY, Kim ES. Targeted therapies in squamous cell carcinoma of the head and neck. Cancer 2009;115:922–35.

[3] Hardisson D. Molecular pathogenesis of head and neck squamous cell carcinoma. Eur Arch Otorhinolaryngol 2003;260:502–8.

[4] Yarbrough WG, Slebos RJ, Liebler D. Proteomics: clinical applications for head and neck squamous cell carcinoma. Head Neck 2006;28:549–58.

[5] Srinivas PR, Verma M, Zhao Y, Srivastava S. Proteomics for cancer biomarker discovery. Clin Chem 2002;48:1160–9.

[6] Tomonaga T, Matsushita K, Yamaguchi S, Oh-Ishi M, Kodera Y, Maeda T, et al. Identification of altered protein expression and post-translational modifications in primary colorectal cancer by using agarose two-dimensional gel electrophoresis. Clin Cancer Res 2004;10:2007–14.

[7] Nishimori T, Tomonaga T, Matsushita K, Oh-Ishi M, Kodera Y, Maeda T, et al. Proteomic analysis of primary esophageal squamous cell carcinoma reveals downregulation of a cell adhesion protein, periplakin. Proteomics 2006;6:1011–8.

[8] Seimiya M, Tomonaga T, Matsushita K, Sunaga M, Oh-Ishi M, Kodera Y, et al. Identification of novel immunohistochemical tumor markers for primary hepatocellular carcinoma; clathrin heavy chain and formiminotransferase cyclodeaminase. Hepatology 2008;48:519–30.

[9] Wu D, Matsushita K, Matsubara H, Nomura F, Tomonaga T. An alternative splicing isoform of eukaryotic initiation factor 4H promotes tumorigenesis in vivo and is a potential therapeutic target for human cancer. Int J Cancer 2011;128: 1018–30.

[10] Karp NA, Kreil DP, Lilley KS. Determining a significant change in protein expression with DeCyder during a pair-wise comparison using two-dimensional difference gel electrophoresis. Proteomics 2004;4:1421–32.

[11] Hu Y, Malone JP, Fagan AM, Townsend RR, Holtzman DM. Comparative proteomic analysis of intra- and interindividual variation in human cerebrospinal fluid. Mol Cell Proteomics 2005;4:2000–9.

[12] Mercurio AM, Rabinovitz I, Shaw LM. The alpha 6 beta 4 integrin and epithelial cell migration. Curr Opin Cell Biol 2001;13:541–5.

[13] Lipscomb EA, Mercurio AM. Mobilization and activation of a signaling competent alpha6beta4integrin underlies its contribution to carcinoma progression. Cancer Metastasis Rev 2005;24:413–23.

[14] Mercurio AM, Rabinovitz I. Towards a mechanistic understanding of tumor invasion–lessons from the alpha6beta 4 integrin. Semin Cancer Biol 2001;11:129–41.

[15] Osmanagic-Myers S, Gregor M, Walko G, Burgstaller G, Reipert S, Wiche G. Plectin-controlled keratin cytoarchitecture affects MAP kinases involved in cellular stress response and migration. J Cell Biol 2006;174:557–68.

[16] Janda E, Lehmann K, Killisch I, Jechlinger M, Herzig M, Downward J, et al. Ras and TGF[beta] cooperatively regulate epithelial cell plasticity and metastasis: dissection of Ras signaling pathways. J Cell Biol 2002;156:299–313.

[17] Chakraborti S, Mandal M, Das S, Mandal A, Chakraborti T. Regulation of matrix metalloproteinases: an overview. Mol Cell Biochem 2003;253:269–85.

[18] Whyte J, Bergin O, Bianchi A, McNally S, Martin F. Key signalling nodes in mammary gland development and cancer. Mitogen-activated protein kinase signalling in experimental models of breast cancer progression and in mammary gland development. Breast Cancer Res 2009;11:209.

[19] Hazan RB, Phillips GR, Qiao RF, Norton L, Aaronson SA. Exogenous expression of N-cadherin in breast cancer cells induces cell migration, invasion, and metastasis. J Cell Biol 2000;148:779–90.

[20] Hulit J, Suyama K, Chung S, Keren R, Agiostratidou G, Shan W, et al. N-cadherin signaling potentiates mammary tumor metastasis via enhanced extracellular signal-regulated kinase activation. Cancer Res 2007;67:3106–16.

[21] Kurokawa A, Nagata M, Kitamura N, Noman AA, Ohnishi M, Ohyama T, et al. Diagnostic value of integrin alpha3, beta4, and beta5 gene expression levels for the clinical outcome of tongue squamous cell carcinoma. Cancer 2008;112:1272–81.

[22] Mattijssen V, Peters HM, Schalkwijk L, Manni JJ, van 't Hof-Grootenboer B, de Mulder PH, et al. E-cadherin expression in head and neck squamous-cell carcinoma is associated with clinical outcome. Int J Cancer 1993;55: 580–5.

[23] Bowie GL, Caslin AW, Roland NJ, Field JK, Jones AS, Kinsella AR. Expression of the cell-cell adhesion molecule E-cadherin in squamous cell carcinoma of the head and neck. Clin Otolaryngol Allied Sci 1993;18:196–201.

[24] Takes RP, Baatenburg De Jong RJ, Alles MJ, Meeuwis CA, Marres HA, Knegt PP, et al. Markers for nodal metastasis in head and neck squamous cell cancer. Arch Otolaryngol Head Neck Surg 2002;128:512–8.

[25] Boczonadi V, McInroy L, Maatta A. Cytolinker cross-talk: periplakin N-terminus interacts with plectin to regulate keratin organisation and epithelial migration. Exp Cell Res 2007;313:3579–91.

[26] Rezniczek GA, de Pereda JM, Reipert S, Wiche G. Linking integrin alpha6beta4-based cell adhesion to the intermediate filament cytoskeleton: direct interaction between the beta4 subunit and plectin at multiple molecular sites. J Cell Biol 1998;141:209–25.

[27] Chao C, Lotz MM, Clarke AC, Mercurio AM. A function for the integrin alpha6beta4 in the invasive properties of colorectal carcinoma cells. Cancer Res 1996;56:4811–9.

[28] Lu S, Simin K, Khan A, Mercurio AM. Analysis of integrin beta4 expression in human breast cancer: association with basal-like tumors and prognostic significance. Clin Cancer Res 2008;14:1050–8.

[29] Huang C, Jacobson K, Schaller MD. MAP kinases and cell migration. J Cell Sci 2004;117:4619–28.

[30] Ding Y, Zhang L, Goodwin JS, Wang Z, Liu B, Zhang J, et al. Plectin regulates the signaling and trafficking of the HIV-1 co-receptor CXCR4 and plays a role in HIV-1 infection. Exp Cell Res 2008;314:590–602.

[31] Kaifi JT, Yekebas EF, Schurr P, Obonyo D, Wachowiak R, Busch P, et al. Tumor-cell homing to lymph nodes and bone marrow and CXCR4 expression in esophageal cancer. J Natl Cancer Inst 2005;97:1840–7.

[32] Muller A, Homey B, Soto H, Ge N, Catron D, Buchanan ME, et al. Involvement of chemokine receptors in breast cancer metastasis. Nature 2001;410:50–6.

[33] Yasumoto K, Koizumi K, Kawashima A, Saitoh Y, Arita Y, Shinohara K, et al. Role of the CXCL12/CXCR4 axis in peritoneal carcinomatosis of gastric cancer. Cancer Res 2006;66:2181–7.

[34] Koshiba T, Hosotani R, Miyamoto Y, Ida J, Tsuji S, Nakajima S, et al. Expression of stromal cell-derived factor 1 and CXCR4 ligand receptor system in pancreatic cancer: a possible role for tumor progression. Clin Cancer Res 2000;6:3530–5.

[35] Katayama A, Ogino T, Bandoh N, Nonaka S, Harabuchi Y. Expression of CXCR4 and its down-regulation by IFN-gamma

in head and neck squamous cell carcinoma. Clin Cancer Res 2005;11:2937–46.
[36] Barbero S, Bonavia R, Bajetto A, Porcile C, Pirani P, Ravetti JL, et al. Stromal cell-derived factor 1alpha stimulates human glioblastoma cell growth through the activation of both extracellular signal-regulated kinases 1/2 and Akt. Cancer Res 2003;63:1969–74.
[37] Tan CT, Chu CY, Lu YC, Chang CC, Lin BR, Wu HH, et al. CXCL12/CXCR4 promotes laryngeal and hypopharyngeal squamous cell carcinoma metastasis through MMP-13-dependent invasion via the ERK1/2/AP-1 pathway. Carcinogenesis 2008;29:1519–27.
[38] Brand S, Dambacher J, Beigel F, Olszak T, Diebold J, Otte JM, et al. CXCR4 and CXCL12 are inversely expressed in colorectal cancer cells and modulate cancer cell migration, invasion and MMP-9 activation. Exp Cell Res 2005;310:117–30.
[39] Phillips RJ, Burdick MD, Lutz M, Belperio JA, Keane MP, Strieter RM. The stromal derived factor-1/CXCL12-CXC chemokine receptor 4 biological axis in non-small cell lung cancer metastases. Am J Respir Crit Care Med 2003;167:1676–86.
[40] Hwang JH, Hwang JH, Chung HK, Kim DW, Hwang ES, Suh JM, et al. CXC chemokine receptor 4 expression and function in human anaplastic thyroid cancer cells. J Clin Endocrinol Metab 2003;88:408–16.
[41] Nagle RB, Hao J, Knox JD, Dalkin BL, Clark V, Cress AE. Expression of hemidesmosomal and extracellular matrix proteins by normal and malignant human prostate tissue. Am J Pathol 1995;146:1498–507.
[42] Lee KY, Liu YH, Ho CC, Pei RJ, Yeh KT, Cheng CC, et al. An early evaluation of malignant tendency with plectin expression in human colorectal adenoma and adenocarcinoma. J Med 2004;35:141–9.
[43] Kelly KA, Bardeesy N, Anbazhagan R, Gurumurthy S, Berger J, Alencar H, et al. Targeted nanoparticles for imaging incipient pancreatic ductal adenocarcinoma. PLoS Med 2008;5:e85.
[44] Sonnenberg A, Liem RK. Plakins in development and disease. Exp Cell Res 2007;313:2189–203.
[45] Wiche G. Role of plectin in cytoskeleton organization and dynamics. J Cell Sci 1998;111(Pt 17):2477–86.
[46] Andra K, Nikolic B, Stocher M, Drenckhahn D, Wiche G. Not just scaffolding: plectin regulates actin dynamics in cultured cells. Genes Dev 1998;12:3442–51.
[47] Stegh AH, Herrmann H, Lampel S, Weisenberger D, Andra K, Seper M, et al. Identification of the cytolinker plectin as a major early in vivo substrate for caspase 8 during CD95- and tumor necrosis factor receptor-mediated apoptosis. Mol Cell Biol 2000;20:5665–79.
[48] Cooper JS, Pajak TF, Forastiere AA, Jacobs J, Campbell BH, Saxman SB, et al. Postoperative concurrent radiotherapy and chemotherapy for high-risk squamous-cell carcinoma of the head and neck. N Engl J Med 2004;350:1937–44.
[49] Bernier J, Domenge C, Ozsahin M, Matuszewska K, Lefebvre JL, Greiner RH, et al. Postoperative irradiation with or without concomitant chemotherapy for locally advanced head and neck cancer. N Engl J Med 2004;350:1945–52.
[50] Bernier J, Cooper JS, Pajak TF, van Glabbeke M, Bourhis J, Forastiere A, et al. Defining risk levels in locally advanced head and neck cancers: a comparative analysis of concurrent postoperative radiation plus chemotherapy trials of the EORTC (#22931) and RTOG (# 9501). Head Neck 2005;27:843–50.

JOURNAL OF PROTEOMICS 75 (2012) 833–844

Available online at www.sciencedirect.com

SciVerse ScienceDirect

www.elsevier.com/locate/jprot

Proteomic study of malignant pleural mesothelioma by laser microdissection and two-dimensional difference gel electrophoresis identified cathepsin D as a novel candidate for a differential diagnosis biomarker

Mutsumi Hosako[a], *Taika Muto*[a], *Yukiko Nakamura*[a,f], *Koji Tsuta*[b], *Naobumi Tochigi*[c], *Hitoshi Tsuda*[b], *Hisao Asamura*[d], *Takeshi Tomonaga*[e], *Akira Kawai*[f], *Tadashi Kondo*[a,*]

[a]*Division of Pharmacoproteomics, National Cancer Center Research Institute, Japan*
[b]*Pathology and Clinical Laboratory Division, National Cancer Center Hospital, Japan*
[c]*Pathology Division, National Cancer Center Research Institute, Japan*
[d]*Thoracic Surgery Division, National Cancer Center Hospital, Japan*
[e]*Laboratory of Proteome Research, National Institute of Biomedical Innovation, Japan*
[f]*Division of Musculoskeletal Oncology, National Cancer Center Hospital, Japan*

ARTICLE INFO

Article history:
Received 6 June 2011
Accepted 28 September 2011
Available online 5 October 2011

Keywords:
Malignant pleural mesothelioma
Laser microdissection
Two-dimensional difference gel electrophoresis
Biomarker

ABSTRACT

To investigate the proteomic background of malignancies of the pleura, we examined and compared the proteomic profile of malignant pleural mesothelioma (MPM)(10 cases), lung adenocarcinoma (11 cases), squamous cell carcinoma of the lung (13 cases), pleomorphic carcinoma of the lung (3 cases) and synovial sarcoma (6 cases). Cellular proteins were extracted from specific populations of tumor cells recovered by laser microdissection. The extracted proteins were labeled with CyDye DIGE Fluor saturation dyes and subjected to two-dimensional difference gel electrophoresis (2D-DIGE) using a large format electrophoresis device. Among 3875 protein spots observed, the intensity of 332 was significantly different (Wilcoxon p value less than 0.05) and with more than two-fold inter-sample-group average difference between the different histology groups. Among these 332, 282 were annotated by LC–MS/MS and included known biomarker proteins for MPM, such as calretinin, as well as proteins previously uncharacterized in MPM. Tissue microarray immunohistochemistry revealed that the expression of cathepsin D was lower in MPM than in lung adenocarcinoma (15% vs. 44% of cases respectively in immunohistochemistry). In conclusion, we examined the protein expression profile of MPM and other lung malignancies, and identified cathepsin D to distinguish MPM from most popular lung cancer such as lung adenocarcinoma.

1. Introduction

Malignant pleural mesothelioma (MPM) is considered an almost incurable tumor, showing resistance to chemo- and radiotherapy, and the median survival remains 8 to 18 months [1,2]. Approximately 10,000 to 15,000 MPM cases are newly diagnosed annually worldwide. The incidence of the disease is rising, probably because its etiology is associated with prior exposure to asbestos, which has been widely used as construction material worldwide. Because of the lack of specific clinical symptoms

* *Corresponding author at:* Division of Pharmacoproteomics, National Cancer Center Research Institute, 5-1-1 Tsukiji, Chuo-ku, Tokyo 104-0045, Japan. Tel.: +81 3 3542 2511x3004; fax: +81 3547 5298.
E-mail address: takondo@ncc.go.jp (T. Kondo).

1874-3919/$ – see front matter © 2011 Elsevier B.V. All rights reserved.
doi:10.1016/j.jprot.2011.09.026

as well as diagnostic biomarkers, early diagnosis and differential diagnosis between MPM and other pleural malignancies are often difficult [3,4].

Global genetic studies have revealed the unique molecular background of MPM. Chromosomal aberrations including the frequent loss of chromosome 22 [5] and structural rearrangements of 1p, 3p, 9p and 6q [6,7] were identified by karyotyping and comparative genomic hybridization analyses. Genetic studies revealed frequent inactivation, mutation and down-regulation of tumor suppressor genes such as p16 [8], p14 [9] and NF2-netrin [10]. Aberrantly methylated genes such as TMEM30B, KAZALD1 and MAPL13 were demonstrated by global methylation analyses for CpG islands [11], while transcriptome sequencing revealed mutations in XRCC6, PDZK1IP1, ACTR1A and AVEN in MPM [12]. These studies furthered our understanding of the genetic background of MPM and may lead to clinical applications that will improve the clinical outcome for MPM patients.

Previous studies have also shown that MPM is characterized by the immunohistochemical expression of epithelial membrane antigen, calretinin, WT1, cytokeratin 5/6, HBME-1 and mesothelin [3,4]. Although these immunohistochemical biomarkers may help in the differential diagnosis of MPM to some degree, novel biomarkers with higher sensitivity and specificity have also been long required. Proteomic studies on MPM conducted to date have used tissue microarray samples [13], plasma samples, pleural effusions [14] and cell lines [15–19], none however, has used direct protein extracts from surgical specimens of MPM, probably because MPM has a complex histology and clinical materials are difficult to obtain.

In this paper, we report the proteins that distinguish MPM from the other lung and pleural malignancies, with the aim of developing differential diagnostic biomarkers. We compared the proteome of MPM with that of malignancies that may occur on the pleura and are therefore included in the differential diagnosis of MPM; these include lung adenocarcinoma, squamous cell carcinoma of the lung, pleomorphic carcinoma of the lung and synovial sarcoma. As the tumor tissues of these malignancies include various types of cells, laser microdissection was employed to recover specific tumor cell populations and thus allow accurate protein expression profiling. A combination of two-dimensional difference gel electrophoresis (2D-DIGE) and mass spectrometry was used to identify proteins unique to MPM tissues. Finally, we validated the expression of cathepsin D in MPM and lung adenocarcinoma using tissue microarrays.

2. Materials and methods

2.1. Materials

Surgical specimens were obtained from patients with pleural malignancy, who were subjected to tumor resection with curative intent at the National Cancer Center Hospital between 1998 and 2007. Primary tumor tissues from MPM (10 cases), synovial sarcoma (6 cases), lung adenocarcinoma (11 cases), lung squamous cell carcinoma (13 cases), and lung pleomorphic carcinoma (three cases) were included in the study. The tumor tissues were frozen at −80° at a time of pathological diagnosis, and embedded in O.C.T. compound before laser microdissection. The clinico-pathological data are summarized in Supplementary Table 1. Tissue microarrays were created using tumor tissues of MPM (46 cases) and lung adenocarcinoma (150 cases). This study was approved by the ethical committee of the National Cancer Center, and written informed consent was obtained from all patients involved.

2.2. Laser microdissection and protein extraction

Specific tumor cell populations were recovered from frozen tissues by laser microdissection as described in our previous report [20]. In brief, tissues embedded in O.C.T. were sectioned using a cryostat (CM3050S, Leica, Wetzlar, Germany), and placed onto the membrane of aluminum-framed plates for laser microdissection (Molecular Machines & Industries, Zurich, Switzerland). The tissues were stained with hematoxylin and eosin and examined to confirm the diagnosis and the presence of tumor cells. The neighboring sections were stained with hematoxylin alone, and specific cell populations were recovered under microscopic observation using a laser microdissection machine (mmiCellcut, Molecular Machines & Industries). Approximately 3000 cells were harvested from each sample for one 2D image, which included 3875 protein spots. The proteins were extracted in a urea lysis buffer containing 7 M urea, 2 M thiourea, 3% CHAPS, 2% Triton X-100, and stored at −80° until use.

2.3. 2D-DIGE

For quantitative expression studies, we employed 2D-DIGE using our original large format electrophoresis device, the separation dimension of which is 24 cm × 33 cm, as described in our previous report [21]. In brief, an equal portion of all protein samples was mixed together to create an internal control sample. The internal control sample was labeled with a Cy3 fluorescent dye (CyDye DIGE Fluor saturation dye, GE, Uppsala, Sweden) according to the manufacturer's instruction. Individual samples were labeled with a Cy5 florescent dye (CyDye DIGE Fluor saturation dye). These differently labeled samples were mixed together and separated by 2D-PAGE. The first dimension separation was performed using IPG Dry strip gels (24 cm length, pI range between 4 and 7) with Multiphor II (GE). The second dimension separation was carried out using our original large format electrophoresis device, with a separation distance of 33 cm. After gel electrophoresis, the gels sandwiched between low-fluorescent glass plates were scanned by a laser scanner (Typhoon Trio, GE) at the appropriate wavelength for Cy3 or Cy5. For preparative purposes, 100 μg of protein sample was prepared from homogenized tissues, labeled with Cy3 fluorescent dye and separated by 2D-PAGE. Although the percentage of tumor cells in the tumor tissues was not determined, it is typically 20–80% according to the microscopic observations, depending on the type of malignancies and cases.

2.4. Image analysis and statistical studies

The images were examined with the Progenesis SameSpots (Non-linear Dynamics, Newcastle, UK) image analysis

software. The intensity of the protein spots was measured, and the Cy5 intensity of the protein spots was normalized by the Cy3 intensity for the matched protein spots in the identical gel. The normalized spot intensities were averaged between the data obtained from duplicate or triplicate gels of identical samples. The numerical data set was exported from Progenesis SameSpots as an XML file, and imported to the Expressionist (GeneData, Zurich, Switzerland) data-mining software. We selected the protein spots the intensity of which was statistically significantly different (p value less than 0.05) and showed more than 2 fold differences in average between the sample groups.

2.5. *Mass spectrometric protein identification*

The proteins corresponding to the protein spots were identified by LC–MS/MS as described in our previous report [21]. In brief, the protein spots were localized on the image of the preparative gel, and the spot localization data were recorded as a text file by Progenesis SameSpots. Based on these data and using our original automated spot recovery machine MolecularHunter (AsOne, Osaka, Japan), the target spots were recovered into 96 well plates. In-gel digestion was achieved as described in our previous report [21]. The trypsin digests were subjected to liquid chromatography coupled with tandem mass spectrometry (Finnigan LTQ linear ion trap mass spectrometer, Thermo Electron Co., San Jose, CA) equipped with a nano-electrospray ion source (AMR Inc., Tokyo, Japan). The Mascot software (version 2.1, Matrix Science, London, UK) was used to search for the mass of the peptide ion peaks against the SWISS-PROT database. Proteins with a Mascot score of 35 or more were used for protein identification. When multiple proteins were identified in a single spot, the proteins with the highest number of peptides were considered as those corresponding to the spot.

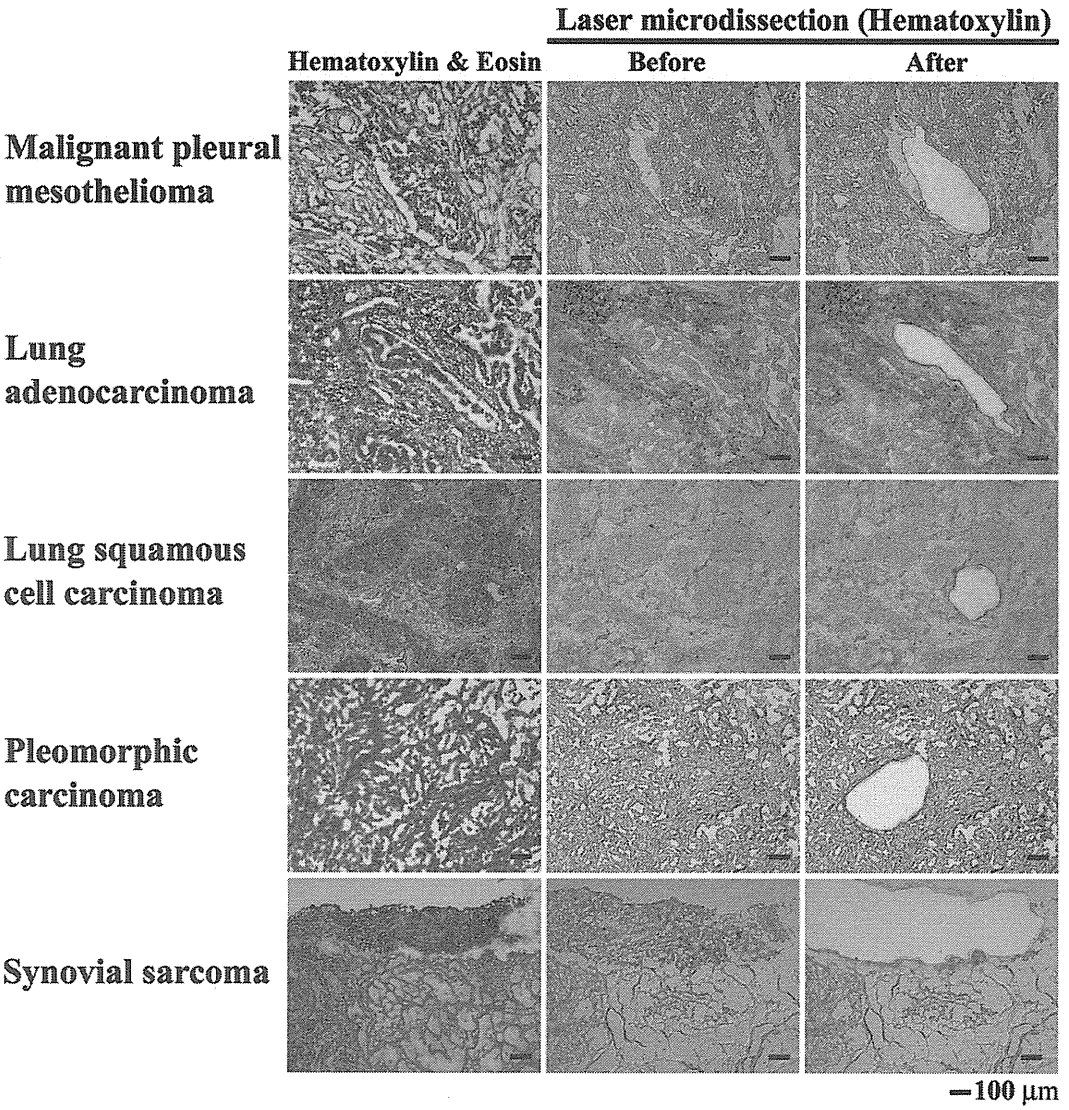

Fig. 1 – Laser microdissection of lung and pleural tumors. The first section was stained with hematoxylin and eosin to confirm the presence of tumor cells. Subsequently, following sections were stained with hematoxylin alone and subjected to laser microdissection. Approximately 3000 cells were harvested to produce one 2D image.

2.6. *Western blotting*

Proteins were separated according to their molecular weight by SDS-PAGE and subsequently blotted on a nitrocellulose membrane. The separated proteins were reacted with antibodies to 14-3-3 sigma (mouse, 1:500; ab11146, Abcam, Cambridge, UK), HSP90 (mouse, 1:1000; 610418, Becton Dickinson, Franklin Lakes, NJ), annexin I (mouse, 1:5000; 610066, Becton Dickinson), cathepsin D (mouse, 1:1000; sc-13148, Santa Cruz, Santa Cruz, CA), ceruloplasmin (rabbit, 1:1000; 611488, Sigma-Aldrich, St. Louis, MO), mimecan (HPA013132, Sigma-Aldrich), pyruvate dehydrogenase kinase isozyme 1 (rabbit, 1:500; 3944-200, Biovision, San Francisco, CA), actin (mouse, 1:250; A5060, Sigma), and horseradish peroxidase-conjugated secondary antibodies for mouse IgG (1:1000; NA931V, GE) and rabbit IgG (1:1000; NA9340V, GE). The immunocomplex was detected by the enhanced chemiluminescence system (ECL Plus, GE) and recorded using LAS-3000 (Fuji Photo Film, Tokyo, Japan).

2.7. *Tissue microarray*

The most representative tumor areas were sampled with a tissue-arraying instrument (Azumaya, Tokyo, Japan) to assemble tissue microarrays (TMAs). To reduce sampling bias due to tumor heterogeneity, we used duplicate samples 2.0 mm in diameter.

For immunohistochemical staining, we deparaffinized 4-μm thick sections from the TMA block. The sections were exposed to 3% hydrogen peroxide for 15 min to block endogenous peroxidase activity and then washed in deionized water for 2–3 min. Sections were then incubated with an antibody against cathepsin D (mouse, 1:1000; sc-13148, Santa Cruz), using the

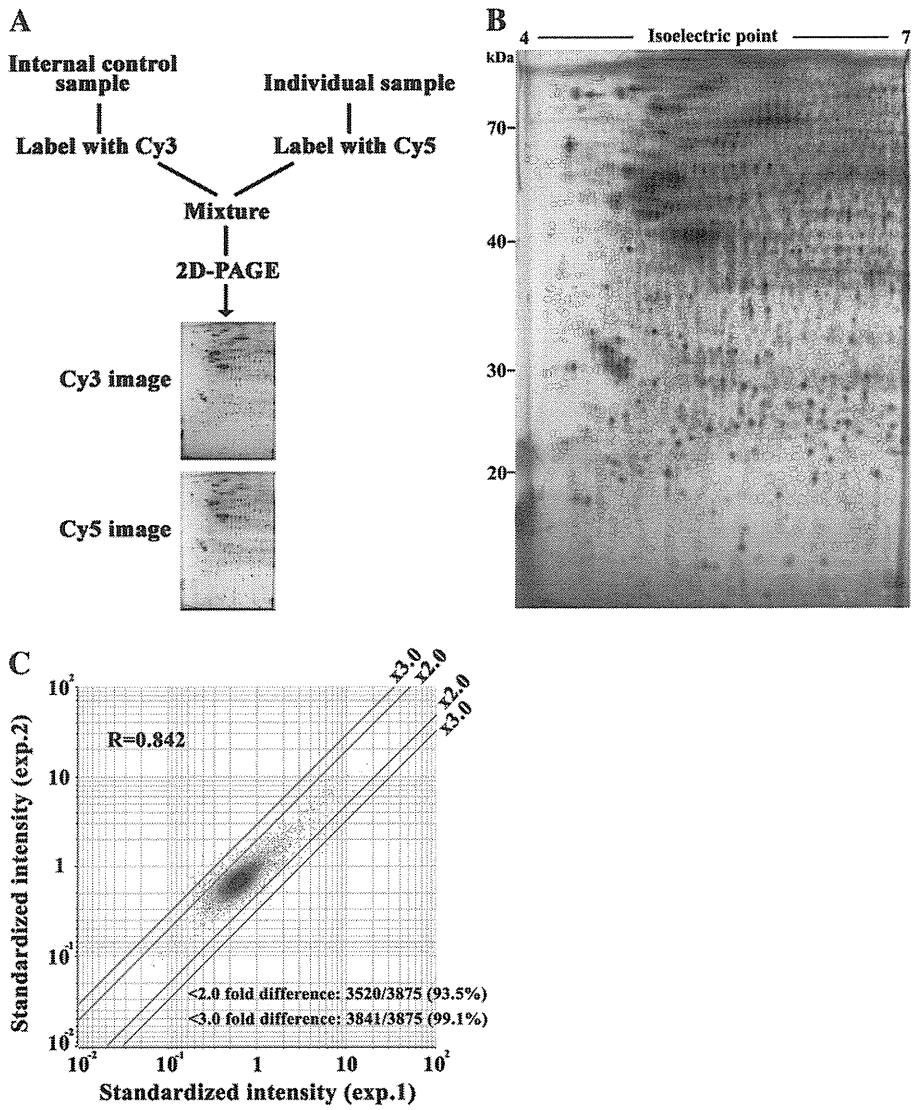

Fig. 2 – Flow of 2D-DIGE experiments. A. The internal control sample and individual samples were labeled with Cy3 and Cy5 CyDye DIGE Fluor saturation dye respectively, and separated by 2D-PAGE. B. A typical 2D gel image. Note that the protein spots were clearly separated, and there was no streaking in the entire gel. C. Scatter gram demonstrating the high system reproducibility achieved. Note that the intensity of 94.5% of the protein spots was scattered within a 2-fold difference range when identical samples were examined twice.

ChemMate EnVisionTM (DAKO) detection method. We used an automated stainer (Dako, Carpinteria, CA), following the vendor's protocol.

The sections were evaluated microscopically for immunoreactivity to cathepsin D by a certified pathologist (K. T.). The cytoplasmic staining intensity was scored using the following system: 0, negative; 1, weak intensity, with observable immunoreactivity only at ×100 magnification; 2, moderate intensity with immunoreactivity easily detected at ×40 magnification but less intense than that of the positive control; 3, intensity equal or stronger than that of the positive control. Furthermore, we evaluated the percentage (0–100%) of tumor cells stained. Next, the staining score per core was obtained by multiplying the intensity score with the percentage of tumor cells stained in each core, its value range being 0–300. The mean of the staining scores obtained in the cores scored per case was used as the staining score for each case. We defined as positive cases with a mean staining score more than 30.

3. Results

Modalities that will aid differential diagnosis continue to be in urgent need, and the identification of biomarkers for MPM may lead to such diagnostic modalities. As the proteome is a functional translation of the genome, regulating the malignant phenotypes of tumor cells, research strategies employing a proteomic approach are among the most promising for biomarker identification and development. However, there has been no report of successful protein expression profiling using direct protein extracts from tumor tissues, one of the major reasons being the complexity of tumor tissues.

Tumor tissues are generally composed of various types of tumor and non-tumor cells. Once they are homogenized for protein extraction, it is hard to identify the origin of the cells from which the proteins derived. The proteome profile of homogenized tissues may reflect two factors: the ratio of the different types of cells in the tissues, and the protein contents of the individual cells. Therefore, accurate or reproducible profiling of homogenized tissues cannot be expected, when the histology is heterogenous and the tumor component varies among samples. To address these problems, we employed laser microdissection to recover specific cell populations before protein extraction (Fig. 1). We have originally reported the use of highly-sensitive fluorescent dyes (CyDye DIGE Fluor saturation dye) for laser microdissected tissues [20]. The use of 2D-DIGE and CyDye DIGE Fluor saturation dyes can generate protein expression profiles even when using a

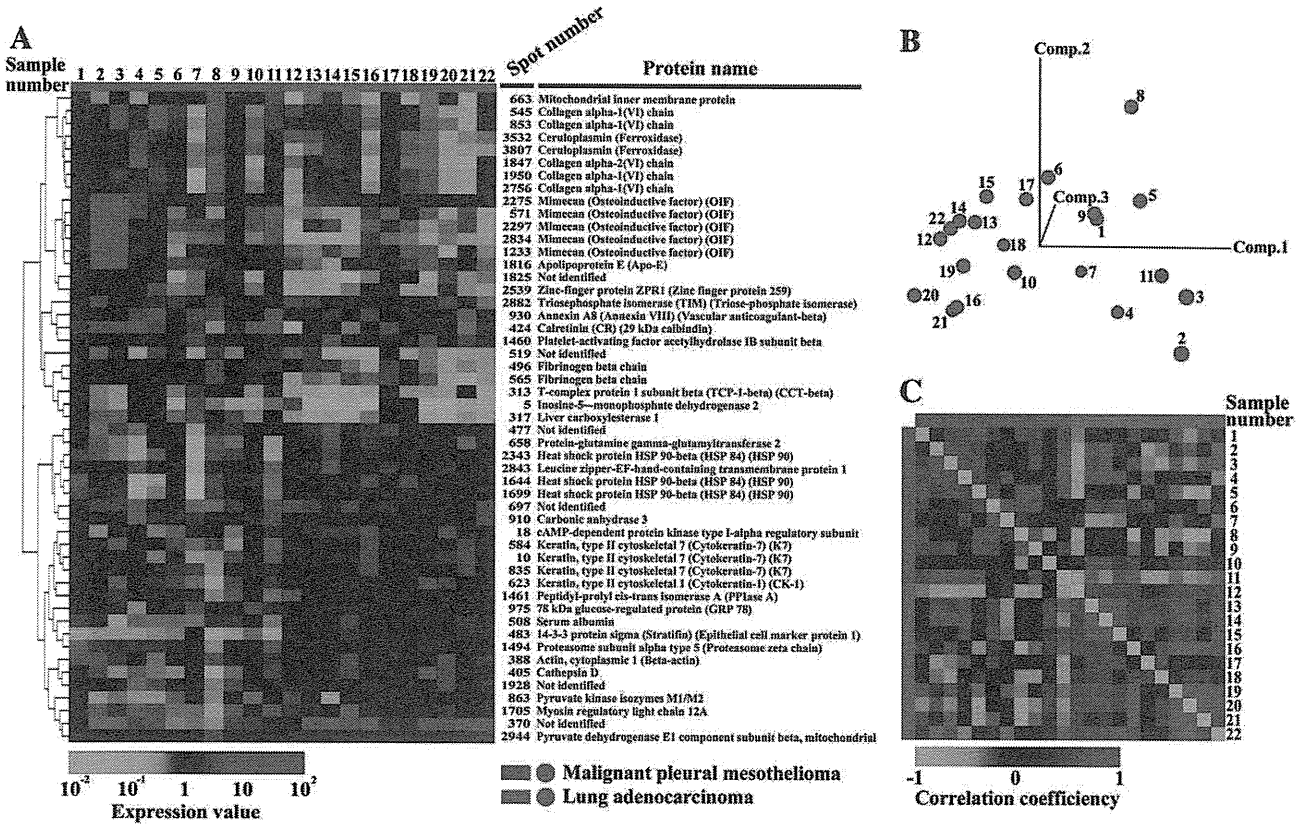

Fig. 3 – 51 Protein spots showed different intensity between the MPM and lung adenocarcinoma groups. A. The intensity of the 51 spots is demonstrated as a heat-map. 28 and 23 spots had higher and lower intensity respectively in MPM than in lung adenocarcinoma. B. Principal component analysis showed that the tumor groups were divided based on the intensity of these protein spots. C. The correlation coefficiency of the 51 protein spots is exhibited as a color-coded matrix. Note that the similarities of the proteome of samples in the same histology group were higher than between samples in different histology groups. The sample numbers correspond to those in Supplementary Table 1.

number of cells as small as 3000 with our original large format electrophoresis device.

2D-DIGE using laser microdissected tissue samples demonstrated high reproducibility in the present, as in previous [22–24], studies. In 2D-DIGE, all gels can generate a 2D image of the common internal control sample, which is a mixture of all protein samples (43 in this study) (Fig. 2A). The image of the internal control sample includes all protein spots observed in individual samples. Mixtures of the fluorescently-labeled internal control sample and individual samples were separated using a large format electrophoresis device, resulting in the observation of 3875 protein spots (Fig. 2B). The protein spots were clearly demarcated, and no remarkable streaking was observed in the entire gel area (Fig. 2B). System reproducibility was examined by running identical samples three times (Fig. 2C). Among the 3875 protein spots observed, the intensity value of more than 93.5% spots was scattered within a twofold difference range, and the correlation coefficiency value (R value) was 0.842 (Fig. 2C). This degree of reproducibility is very high and close to those obtained in our previous proteomic studies using the same 2D-DIGE system [22–24].

The overall features of the proteome were examined by unsupervised classification using the obtained spot intensity values. Hierarchical clustering revealed that most protein samples were grouped according to their histological classification, when they were classified based on the intensity of all protein spots examined (Supplementary Fig. 1A). Visual inspection of the corresponding heat-map showed homogeneity of spot intensity within each sample group. Similar results were obtained when the protein samples were grouped following principal component analysis; again, the samples tended to be grouped according to their histology (Supplementary Fig. 1B). The similarity of the proteome between samples was further demonstrated by illustrating the correlation coefficiency of all pairs of protein spots as a color-coded map, the correlation matrix (Supplementary Fig. 1C). Protein samples with the same histology had higher correlation coefficiency values. All these results suggested that the overall features of the proteome reflect the corresponding histology, demonstrating the possibility of identifying proteins unique to a particular histological classification type through proteomic studies. These results are concordant with our previous studies on lymphoid leukemia [25], soft-tissue sarcoma [26], esophageal cancer [24], and liver cancer [23] using 2D-DIGE, in which the overall proteomic profile reflected histological characteristics.

Non-small cell lung carcinoma (NSCLC) accounts for approximately 85% of lung cancer cases, and 40% of them are adenocarcinomas [27]. Differentiating MPM from lung adenocarcinoma frequently poses a diagnostic challenge, particularly when the tumor has invaded the pleura. We identified 51 protein spots the intensity of which was unique to a particular histological type involved in the differential diagnosis of MPM. The intensity of these protein spots was statistically significantly different (p value less than 0.05) and showed more than two-fold differences between the sample groups. [PL19] The relative intensity of the protein spots is shown as a heat-map (Fig. 3A). The protein identification data are summarized in Supplementary Table 2. The identified proteins included known biomarkers for MPM, such as calretinin (spot 424) (Fig. 3A [PL20]). In addition, this study

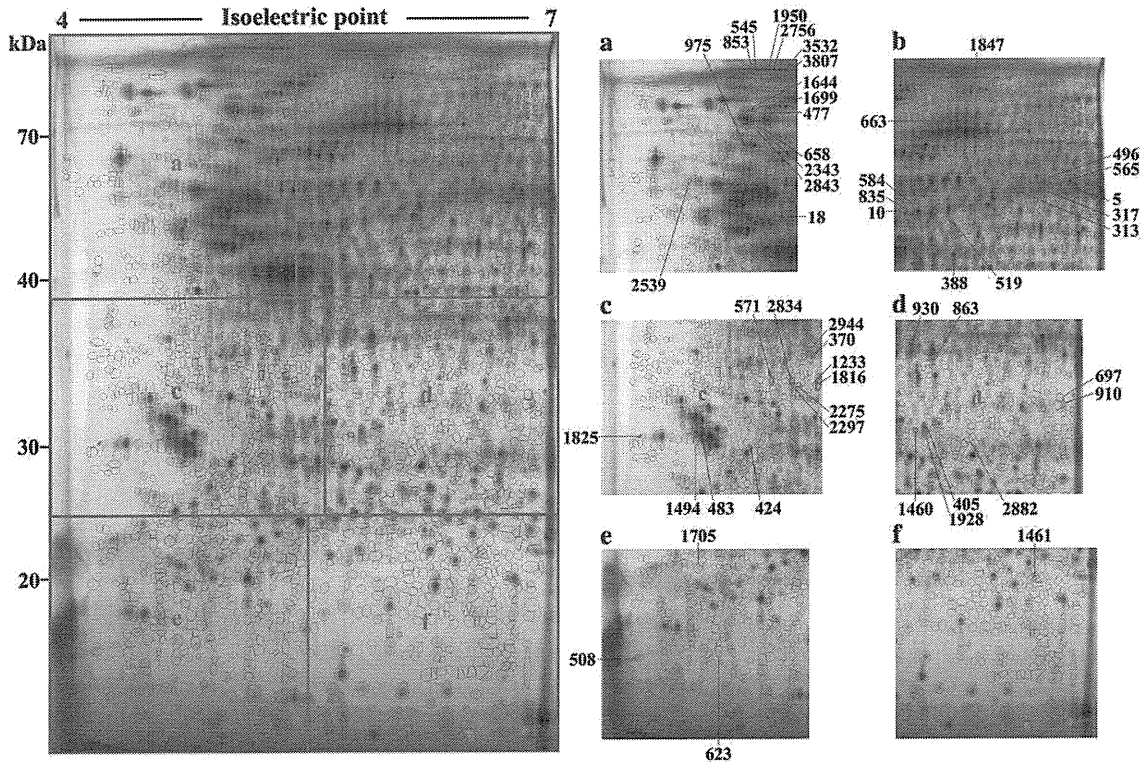

Fig. 4 – Localization of the 51 protein spots with different intensity between the MPM and lung adenocarcinoma samples on the 2D gel.

identified annexin A8, platelet activating factor, vimentin, zinc-finger protein ZPR1, mimecan, fibrinogen, T-complex protein 1, inosine-5-monophosphate dehydrogenase 2, liver carboxylesterase 1, osteonectin, ceruloplasmin, and collagens [WU21] as differentially expressed in the MPM group. Multiple proteins appeared in different protein spots, probably because of post-translational modifications. The protein sample groups were fairly divided according to their profiles based on the set of 51 spots in principal component analysis (Fig. 3B); the similarity of these profiles is shown in the correlation matrix (Fig. 3C). The localization of the identified proteins on the gel is shown in Fig. 4.

Similarly, pair-wise comparisons between MPM and other malignancies identified a number of differentially expressed proteins. The results of comparative studies between MPM and lung squamous cell carcinoma (Supplementary Figs. 2 and 3), MPM and lung pleomorphic carcinoma (Supplementary Figs. 4 and 5), and MPM and synovial sarcoma (Supplementary Figs. 6 and 7) are also shown in heat-maps, principal component analysis graphs and correlation matrices (Supplementary Figs. 2, 4, and 6), and the localization of the protein spots is shown on 2D maps (Supplementary Figs. 3, 5, and 7). The protein identification data are summarized in Supplementary Table 2. We deposited these proteome data in our original open-access proteome database, the Genome Medicine Database of Japan Proteomics [28].

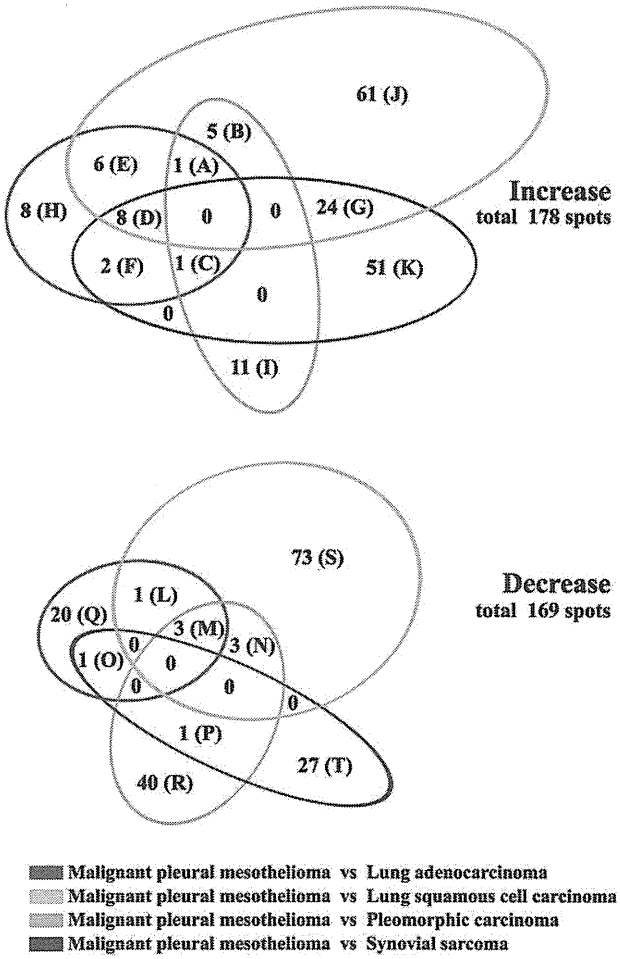

Fig. 5 – Venn diagram of protein spots with different intensity between MPM and the other malignancies examined. The number of protein spots the intensity of which increased or decreased in MPM tissues compared with the other malignancies is shown in the Venn diagrams in upper and lower panels, respectively. The letter in brackets corresponds to the category in Table 1, where the proteins are listed with their spot number and accession number.

We detected a number of protein spots that repeatedly had different intensity between MPM and other malignancies (Fig. 5, Table 1). There was no protein spot whose intensity increased both in MPM and in any other tumor type examined.

The differential expression of the identified proteins was examined by western blotting (Fig. 6). Although we examined seven proteins, only cathepsin D showed western blotting results consistent with the 2D-DIGE data. This discordance between 2D-DIGE and western blotting results may be due to the presence of multiple isoform spots that did not have significantly different intensity between MPM and the other tumor types. It is also possible that the antibodies used recognize different isoforms from those observed in 2D-DIGE, resulting in discordant results between 2D-DIGE and western blotting.

We further validated the expression of cathepsin D in MPM and lung adenocarcinoma. TMA immunohistochemistry revealed that positive expression of cathepsin D was observed in a significantly lower number of cases in MPM (15%, 7/46 cases) compared with lung adenocarcinoma (44%, 66/150 cases) (χ^2 test, $p=0.0004$).

4. Discussion

We demonstrated that the combination of laser microdissection technique with 2D-DIGE, one of the most popular proteomic modalities, enabled the identification of proteins unique to histologically different lung cancers. Total number of protein species observed in this study was 3875, which may be quite large considering that the samples were obtained by laser microdissection. The approach in this study could be applicable to any types of malignant tumors. We also demonstrated the utilities of TMA for validation study. Because immunohistochemistry could be considered as a routine clinical examination, the results obtained by TMA may be directly applicable to the clinical setting.

The number of samples in this study was quite limited, as the incidence of MPM is relatively small and most of the patients with MPM visit the hospital when the tumors fully developed and the patients are not operative. This is the inherent problem of the global expression study on the rare cancers. The limited number of samples may affect the results of comparative studies. Although the expression of cathepsin D was statistically different between MPM and lung adenocarcinoma, as our study represents a small validation study, a diagnostic power of cathepsin D should be further validated in a large scale sample set.

While the expression of cathepsin D has not been previously reported in MPM, it has in non-small lung carcinoma [29]. The percentage of cathepsin D positive cases in lung adenocarcinoma was concordant with that reported in a previous study [29]. Up-regulation of cathepsin D has also been reported in a highly

Table 1 – List of identified proteins and spot numbers on Venn diagram.

Spot no.	Accession no.	Identified protein
Proteins in category A		
663	Q16891	Mitochondrial inner membrane protein
Proteins in category B		
743		Not identified
833	P08758	Annexin A5
1528	P12110	Collagen alpha-2(VI) chain
1629	P06396	Gelsolin
1818	Q16555	Dihydropyrimidinase-related protein 2
Proteins in category C		
930	P13928	Annexin A8
Proteins in category D		
424	P22676	Calretinin
545	P12109	Collagen alpha-1(VI) chain
571	P20774	Mimecan
1233	P20774	Mimecan
1816	P02649	Apolipoprotein E
1825		Not identified
2297	P20774	Mimecan
2834	P20774	Mimecan
Proteins in category E		
1847	P12110	Collagen alpha-2(VI) chain
1950	P12109	Collagen alpha-1(VI) chain
2275	P20774	Mimecan
2756	P12109	Collagen alpha-1(VI) chain
3532	P00450	Ceruloplasmin
3807	P00450	Ceruloplasmin
Proteins in category F		
5	P12268	Inosine-5~-monophosphate dehydrogenase 2
853	P12109	Collagen alpha-1(VI) chain
Proteins in category G		
431	P40261	Nicotinamide N-methyltransferase
454	O95833	Chloride intracellular channel protein 3
457	O75821	Eukaryotic translation initiation factor 3 subunit 4
479	P20774	Mimecan
540	P08670	Vimentin
581	P08670	Vimentin
582	P20774	Mimecan
585	P09525	Annexin A4
620	P20774	Mimecan
640	P39687	Acidic leucine-rich nuclear phosphoprotein 32 family member A
775	P13645	Keratin, type I cytoskeletal 10
922	P20774	Mimecan
937	Q5H9L2	Transcription elongation factor A protein-like 5
956	P02675	Fibrinogen beta chain
1074		Not identified
1101	P07355	Annexin A2
1108	P12429	Annexin A3
1377	P07910	Heterogeneous nuclear ribonucleoproteins C1/C2
1499		Not identified
1520	P29692	Elongation factor 1-delta
1984	P04264	Keratin, type II cytoskeletal 1
2652	P20774	Mimecan
2653	P51884	Lumican
2873	P50225	Sulfotransferase 1A1

Table 1 *(continued)*

Spot no.	Accession no.	Identified protein
Proteins in category H		
313	P78371	T-complex protein 1 subunit beta
317	P23141	Liver carboxylesterase 1
496	P02675	Fibrinogen beta chain
519		Not identified
565	P02675	Fibrinogen beta chain
1460	P68402	Platelet-activating factor acetylhydrolase IB subunit beta
2539	O75312	Zinc-finger protein ZPR1
2882	P60174	Triosephosphate isomerase
Proteins in category I		
61	P36776	Lon protease homolog, mitochondrial
174	P13010	ATP-dependent DNA helicase 2 subunit 2
299	P02675	Fibrinogen beta chain
825	P22102	Trifunctional purine biosynthetic protein adenosine-3
1612	P68104	Elongation factor 1-alpha 1
1669	P06396	Gelsolin
1867	P06396	Gelsolin
2690	P02768	Serum albumin
3181	P36871	Phosphoglucomutase-1
3196	P35241	Radixin
3490	P09211	Glutathione S-transferase P
Proteins in category J		
40	P82979	Nuclear protein Hcc-1
105	P08670	Vimentin
126	P60709	Actin, cytoplasmic 1
164	Q9H2J4	Phosducin-like protein 3
278		Not identified
288	P68871	Hemoglobin subunit beta
337	P04264	Keratin, type II cytoskeletal 1
338	P04264	Keratin, type II cytoskeletal 1
369	P36952	Serpin B5
375	Q9Y570	Protein phosphatase methylesterase 1
389	P12429	Annexin A3
400	P06748	Nucleophosmin
402	Q16555	Dihydropyrimidinase-related protein 2
416	P09960	Leukotriene A-4 hydrolase
521	P09382	Galectin-1
535	P08670	Vimentin
552	P08670	Vimentin
595	P08670	Vimentin
597	P20774	Mimecan
644	P13645	Keratin, type I cytoskeletal 10
694	P36955	Pigment epithelium-derived factor
714	Q9Y696	Chloride intracellular channel protein 4
746	P08670	Vimentin
805	P37235	Hippocalcin-like protein 1
860	P04264	Keratin, type II cytoskeletal 1
891	P05388	60S acidic ribosomal protein P0
897	P09486	SPARC
974	P20774	Mimecan
1016		Not identified
1238		Not identified
1274		Not identified
1287	P68871	Hemoglobin subunit beta
1317	Q14019	Coactosin-like protein
1414	P68871	Hemoglobin subunit beta
1443	P08670	Vimentin
1500		Not identified
1536	P30040	Endoplasmic reticulum protein ERp29
1574	P20774	Mimecan

Table 1 (continued)

Spot no.	Accession no.	Identified protein
Proteins in category J		
1672	P02545	Lamin-A/C
1747	P12109	Collagen alpha-1(VI) chain
1768		Not identified
1780	P12109	Collagen alpha-1(VI) chain
1861	P02649	Collagen alpha-2(VI) chain
2012	P12110	Collagen alpha-2(VI) chain
2165	P08758	Annexin A5
2193	P02679	Fibrinogen gamma chain
2219		Not identified
2222	P02768	Serum albumin
2236	P02768	Serum albumin
2264	P02768	Serum albumin
2573	P12429	Annexin A3
2602	P08758	Annexin A5
2674	P02768	Serum albumin
2688	P12110	Collagen alpha-2(VI) chain
3182	P12109	Collagen alpha-1(VI) chain
3252		Not identified
3344	P12110	Collagen alpha-2(VI) chain
3401		Not identified
3509		Not identified
3658	P00492	Hypoxanthine-guanine phosphoribosyltransferase
3665		Not identified
Proteins in category K		
67	P02675	Fibrinogen beta chain
235		Not identified
331	331	Ezrin
415		Not identified
425		Not identified
438	P30740	Leukocyte elastase inhibitor
531	P15311	Ezrin
551	P15311	Ezrin
615		Not identified
638		Not identified
679	Q13451	FK506-binding protein 5
684	P47895	Aldehyde dehydrogenase 1A3
723	P48507	Glutamate–cysteine ligase regulatory subunit
830	P52566	Rho GDP-dissociation inhibitor 2
950	P60660	Myosin light polypeptide 6
977	P22676	Calretinin
993	P05787	Keratin, type II cytoskeletal 8
998		Not identified
1058	P06748	Nucleophosmin
1256	P15311	Ezrin
1455	P29692	Elongation factor 1-delta
1531	P04083	Annexin A1
1583		Not identified
1598		Not identified
1622	P30101	Protein disulfide-isomerase A3
1626		Not identified
1714	O14773	Tripeptidyl-peptidase 1
1846		Not identified
1887	P02649	Apolipoprotein E
1902	O43399	Tumor protein D54
1955	P07339	Cathepsin D
1976	P09493	Tropomyosin alpha-1 chain
2054	P22676	Calretinin
2063	P02649	Apolipoprotein E
2066	P02768	Serum albumin
2142	P04264	Keratin, type II cytoskeletal 1

Table 1 (continued)

Spot no.	Accession no.	Identified protein
Proteins in category K		
2379	P29692	Elongation factor 1-delta
2392	P20774	Mimecan
2481	P60174	Triosephosphate isomerase
2576	P13645	Keratin, type I cytoskeletal 10
2624	P06733	Alpha-enolase
2694	Q9UMS0	NFU1 iron-sulfur cluster scaffold homolog, mitochondrial
2930		Not identified
2949	P26038	Moesin
3074		Not identified
3089	Q92688	Acidic leucine-rich nuclear phosphoprotein 32 family member B
3320	P51884	Lumican
3360	O43399	Tumor protein D54
3582		Not identified
3625	P07355	Annexin A2
3868	P04083	Annexin A1
Proteins in category L		
1494	P28066	Proteasome subunit alpha type 5
Proteins in category M		
483	P31947	14-3-3 Protein sigma
508	P02768	Serum albumin
863	P14618	Pyruvate kinase isozymes M1/M2
Proteins in category N		
90	P07195	L-lactate dehydrogenase B chain
268	P06702	Protein S100-A9
1158	P61289	Proteasome activator complex subunit 3
Proteins in category O		
1644	P08238	Heat shock protein HSP 90-beta
Proteins in category P		
3669	O75083	WD repeat protein 1
Proteins in category Q		
10	P08729	Keratin, type II cytoskeletal 7
18	P10644	cAMP-dependent protein kinase type I-alpha regulatory subunit
370		Not identified
388	P60709	Actin, cytoplasmic 1
405	P07339	Cathepsin D
477		Not identified
584	P08729	Keratin, type II cytoskeletal 7
623	P04264	Keratin, type II cytoskeletal 1
658	P21980	Protein-glutamine gamma-glutamyltransferase 2
697		Not identified
835	P08729	Keratin, type II cytoskeletal 7
910	P07451	Carbonic anhydrase 3
975	P11021	78 kDa glucose-regulated protein
1461	P62937	Peptidyl-prolyl cis–trans isomerase A
1699	P08238	Heat shock protein HSP 90-beta
1705	P19105	Myosin regulatory light chain 12A
1928		Not identified
2343	P08238	Heat shock protein HSP 90-beta
2843	O95202	Leucine zipper-EF-hand-containing transmembrane protein 1, mitochondrial
2944	P11177	Pyruvate dehydrogenase E1 component subunit beta, mitochondrial

(continued on next page)

Table 1 (continued)

Spot no.	Accession no.	Identified protein
Proteins in category R		
296	P06702	Protein S100-A9
368	P06748	Nucleophosmin
374	P04632	Calpain small subunit 1
407	P09651	Heterogeneous nuclear ribonucleoprotein A1
506	P02768	Serum albumin
527	P04264	Keratin, type II cytoskeletal 1
574	P02545	Lamin-A/C
647	P08758	Annexin A5
706	P00738	Haptoglobin
817	P07355	Annexin A2
841	P68104	Elongation factor 1-alpha 1
959	P05388	60S Acidic ribosomal protein P0
999	P68104	Elongation factor 1-alpha 1
1020	P63104	14-3-3 Protein zeta/delta
1023	P60709	Actin, cytoplasmic 1
1057	P11142	Heat shock cognate 71 kDa protein
1102	P18206	Vinculin
1121	P07355	Annexin A2
1167	P09211	Glutathione S-transferase P
1275	P04406	Glyceraldehyde-3-phosphate dehydrogenase
1278	O43776	Asparaginyl-tRNA synthetase, cytoplasmic
1308	P14618	Pyruvate kinase isozymes M1/M2
1384	P21964	Catechol O-methyltransferase
1451	P68104	Elongation factor 1-alpha 1
1639	P07355	Annexin A2
1670	P07355	Annexin A2
1722	P02768	Serum albumin
1941	P46109	Crk-like protein
2050	P31948	Stress-induced-phosphoprotein 1
2383	P04264	Keratin, type II cytoskeletal 1
2629		Not identified
2780	P02787	Serotransferrin
2914	P31942	Heterogeneous nuclear ribonucleoprotein H3
2976	P12814	Alpha-actinin-1
3151	Q8WXX5	DnaJ homolog subfamily C member 9
3638	P27824	Calnexin
3736	P27824	Calnexin
3764	P27824	Calnexin
3799	P04264	Keratin, type II cytoskeletal 1
3859	P14625	Endoplasmin
Proteins in category S		
1	P13645	Keratin, type I cytoskeletal 10
2	P55036	26S Proteasome non-ATPase regulatory subunit 4
3	Q12765	Secernin-1
4	Q04695	Keratin, type I cytoskeletal 17
5	P12268	Inosine-5~-monophosphate dehydrogenase 2
6	Q04695	Keratin, type I cytoskeletal 17
9	P11413	Glucose-6-phosphate 1-dehydrogenase
32	P37837	Transaldolase
47		Not identified
73		Not identified
96	O43237	Cytoplasmic dynein 1 light intermediate chain 2
127		Not identified
197	P07195	L-lactate dehydrogenase B chain
263	Q09028	Histone-binding protein RBBP4
267	Q04695	Keratin, type I cytoskeletal 17
269	Q04695	Keratin, type I cytoskeletal 17
272	P55036	26S Proteasome non-ATPase regulatory subunit 4
274	P55036	26S Proteasome non-ATPase regulatory subunit 4

Table 1 (continued)

Spot no.	Accession no.	Identified protein
Proteins in category S		
277	Q09028	Histone-binding protein RBBP4
280	Q12765	Secernin-1 — Homo sapiens (Human)
285	P19338	Nucleolin (Protein C23) — Homo sapiens (Human)
293		Not identified
295	Q13228	Selenium-binding protein 1 — Homo sapiens (Human)
298	P00352	Retinal dehydrogenase 1
299	P02675	Fibrinogen beta chain
302	Q01469	Fatty acid-binding protein, epidermal
304	P00352	Retinal dehydrogenase 1
313	P78371	T-complex protein 1 subunit beta
315	P08670	Vimentin
317	P23141	Liver carboxylesterase 1
319		Not identified
323		Not identified
324	P02675	Fibrinogen beta chain
326	P19338	Nucleolin (Protein C23)
327	P19338	Nucleolin (Protein C23)
330	P78371	T-complex protein 1 subunit beta
333	P12268	Inosine-5~-monophosphate dehydrogenase 2
339		Not identified
348	Q16891	Mitochondrial inner membrane protein
367	P06576	ATP synthase subunit beta, mitochondrial
377	P00352	Retinal dehydrogenase 1
395	P55036	26S Proteasome non-ATPase regulatory subunit 4
403	Q9H4M9	EH domain-containing protein 1
413	Q04760	Lactoylglutathione lyase
415		Not identified
430	P13645	Keratin, type I cytoskeletal 10
465	P04792	Heat-shock protein beta-1
476	O75934	Breast carcinoma amplified sequence 2
481	P04406	Glyceraldehyde-3-phosphate dehydrogenase
500	O94788	Retinal dehydrogenase 2
502	P00488	Coagulation factor XIII A chain
526	P05120	Plasminogen activator inhibitor 2
530		Not identified
578	P09936	Ubiquitin carboxyl-terminal hydrolase isozyme L1
662	P02538	Keratin, type II cytoskeletal 6A
693	P62191	26S Protease regulatory subunit 4
701	P37837	Transaldolase
716	Q01518	Adenylyl cyclase-associated protein 1
726	P50395	Rab GDP dissociation inhibitor beta
745	P31146	Coronin-1A
773	P13645	Transaldolase
783	P13647	Keratin, type II cytoskeletal 5
890	P31943	Heterogeneous nuclear ribonucleoprotein H
938	Q02790	FK506-binding protein 4
945	P08670	Vimentin
1019	P04792	Heat-shock protein beta-1
1118		Not identified
1280	P78371	T-complex protein 1 subunit beta
1340	P37837	Transaldolase
1408	P06396	Gelsolin
1824	P31947	14-3-3 Protein sigma
2433	P62191	26S Protease regulatory subunit 4
2829	P63104	14-3-3 Protein zeta/delta
Proteins in category T		
69	P31943	Heterogeneous nuclear ribonucleoprotein H
74	P55795	Heterogeneous nuclear ribonucleoprotein H~

Table 1 (continued)

Spot no.	Accession no.	Identified protein
Proteins in category T		
135	Q92945	Far upstream element-binding protein 2
147	P13010	ATP-dependent DNA helicase 2 subunit 2
191		Not identified
279	P29762	Cellular retinoic acid-binding protein 1
305	P14625	Endoplasmin
464	O00410	Importin-5
471	Q03252	Lamin-B2
621	P12956	ATP-dependent DNA helicase 2 subunit 1
625	P08107	Heat shock 70 kDa protein 1
635	Q03252	Lamin-B2
654	P12956	ATP-dependent DNA helicase 2 subunit 1
823	P28072	Proteasome subunit beta type 6
887	P04264	Keratin, type II cytoskeletal 1
1155	O60826	Coiled-coil domain-containing protein 22
1205	O75351	Vacuolar protein sorting-associating protein 4B
1587	P37837	Transaldolase
1698	Q9UQ80	Proliferation-associated protein 2G4
1719	P83916	Chromobox protein homolog 1
1822	P08238	Heat shock protein HSP 90-beta
1995	P07339	Heat shock protein HSP 90-beta
2055	P31939	Bifunctional purine biosynthesis protein PURH
2364	P05455	Lupus La protein
2471	P12956	ATP-dependent DNA helicase 2 subunit 1
3012	P61758	Prefoldin subunit 3
3845	Q9Y3Z3	SAM domain and HD domain-containing protein 1

Categories corresponded to those in Fig. 5. The data supportive to protein identification are demonstrated in Supplementary Table 2.
Categories corresponded to those in Fig. 5. The data supportive to protein identification are demonstrated in Supplementary Table 2.

metastatic breast cancer cell line [30], and the inhibition of cathepsin D resulted in significant reduction of in vitro invasion, lung colonization in nude mice, as well as promotion of apoptosis by serum starvation [31]. Although these observations suggest a contribution of cathepsin D to the malignant phenotype is plausible, the molecular backgrounds of the unique expression of cathepsin D in lung adenocarcinoma in comparison with MPM are not clear yet.

5. Conclusions

Using surgically resected tissues and 2D-DIGE, we identified the proteins the expression of which is statistically significantly different between MPM and malignancies that may arise from the pleura. Our report demonstrated the advantages offered by the combined use of laser microdissection and 2D-DIGE with highly sensitive fluorescent dye for diseased tissues with complex histology. We also demonstrated the utilities of TMA for validation study. The identified proteins included established biomarker proteins for MPM such as calretinin. Immunohistochemistry revealed that cathepsin D may be a novel biomarker for differential diagnosis of MPM from lung adenocarcinoma. Further validation studies on the diagnostic utility of cathepsin D in a large number of cases will be of great interest in terms of their potential for the development of novel clinical applications.

Supplementary materials related to this article can be found online at doi:10.1016/j.jprot.2011.09.026.

Acknowledgments

This work was supported by a grant from the Ministry of Health, Labor and Welfare and by the Program for Promotion of Fundamental Studies in Health Sciences of the National Institute of Biomedical Innovation of Japan. We appreciate Dr. Akihiko Yoshida for the useful pathology consultation.

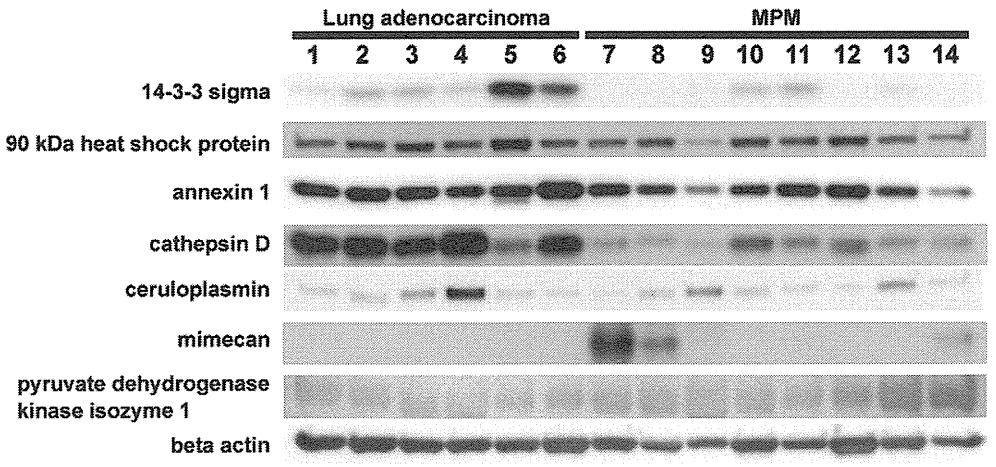

Fig. 6 – Western blotting for the proteins identified by 2D-DIGE study. The expression of seven proteins, the expression of which was different between MPM and lung adenocarcinoma in 2D-DIGE study, was monitored using specific antibodies. Note that cathepsin D showed consistent up-regulation in lung adenocarcinoma. The intensity of protein bands normalized with that of beta-actin is demonstrated in Supplementary Fig. 8.